arXiv:1706.04921v1 [astro-ph.CO] 15 Jun 2017

UT-17-15

Can decaying particle explain cosmic infrared background excess?

Kazunori Kohri[a,b], Takeo Moroi[c,d] and Kazunori Nakayama[c,d]

[a] *Institute of Particle and Nuclear Studies, KEK, 1-1 Oho, Tsukuba, Ibaraki 305-0801, Japan*

[b] *The Graduate University for Advanced Studies (SOKENDAI), 1-1 Oho, Tsukuba, Ibaraki 305-0801, Japan*

[c] *Department of Physics, Faculty of Science, The University of Tokyo, Bunkyo-ku, Tokyo 113-0033, Japan*

[d] *Kavli IPMU (WPI), UTIAS, The University of Tokyo, Kashiwa, Chiba 277-8583, Japan*

Abstract

Recently the CIBER experiment measured the diffuse cosmic infrared background (CIB) flux and claimed an excess compared with integrated emission from galaxies. We show that the CIB spectrum can be fitted by the additional photons produced by the decay of a new particle. However, it also contributes too much to the anisotropy of the CIB, which is in contradiction with the anisotropy measurements by the CIBER and Hubble Space Telescope.

1 Introduction

Origins of the total flux of the diffuse cosmic infrared background (CIB) radiation have not been known for certain. However, it is believed that the CIB should be integrated radiation of photons emitted in the past Universe through the cosmic history. For example, the infrared radiation can be produced at least in standard mechanisms of galaxy formations and evolutions [2]. Therefore, precise observational data are expected to constrain unknown mechanisms in which the CIB are additionally produced, e.g., as relics of redshifted ultraviolet photons emitted at an epoch of cosmic reionization induced by Pop III stars, young galaxies, or black holes [3, 4, 5, 6, 7, 8].

Quite recently the Cosmic Infrared Background Experiment (CIBER) collaboration reported their first result of spectral measurements for the diffuse CIB radiation in unexplored wavelength ranges from $0.8\,\mu$m to $1.7\,\mu$m by their sounding rocket experiments [1]. Remarkably, they found that there exist significant excesses in their data compared with the previous prediction deduced theoretically by indirect observations with counting numbers of galaxies [2]. This discrepancy cannot be resolved even if they adopt a model-independent lower limit on the observed CIB radiation [1]. So far there are no natural astrophysical candidates which explains those excesses of the CIB radiation at around the wavelength $\sim 1\ \mu$m.

In this paper, we study scenarios in which the CIB spectrum is fitted by additional photons produced by a decaying hypothetical particle. However, such a scenario predicts too large CIB anisotropy spectrum, which contradicts with the measurement by the Hubble Space telescope (HST) [9] and CIBER itself [10].

The plan of the paper is as follows. In Sec. 2 we discuss the possibility that the decaying particle explains the excess CIB radiation and constraints from star cooling. In Sec. 3, the CIB anisotropy spectrum in the decaying particle model is studied. It is shown that models to explain the excess in the mean CIB intensity contradicts with the measurement of the CIB anisotropy spectrum. Sec. 4 is devoted to conclusions and discussion.

2 CIB from Decaying Particle

2.1 Mean Intensity from Decaying Particle

Let us suppose that there is a light particle ϕ which decays into another particle χ plus photon γ. For the moment we do not specify the model: ϕ and χ can either be bosons or fermions, which are assumed to be singlets under the standard-model gauge group.

Independently of the detailed model, the CIB spectrum from the ϕ decay can be calculated by the following three parameters: the photon energy produced by the decay ($E_{\rm max}$), the lifetime of ϕ (τ_ϕ) and the abundance of ϕ (Y_ϕ). Here $Y_\phi = n_\phi/s$ denotes the number-to-entropy density ratio of ϕ.[#1] From the kinematics, the photon energy produced by the

[#1] If $\tau_\phi \lesssim t_0$ (t_0 denotes the present age of the universe), n_ϕ/s is not regarded as a constant. We define

decay is given by

$$E_{\rm max} = \frac{m_\phi^2 - m_\chi^2}{2m_\phi}, \tag{1}$$

where m_ϕ and m_χ are masses of ϕ and χ, respectively. For later use we also define r_ϕ, the energy fraction of ϕ in the total dark matter density $\rho_{\rm DM}$,

$$r_\phi \equiv \frac{m_\phi Y_\phi}{\rho_{\rm DM}/s}. \tag{2}$$

Thus Y_ϕ is determined by the combination m_ϕ/r_ϕ. Later we will calculate the CIB spectrum by varying $E_{\rm max}$, τ_ϕ and m_ϕ/r_ϕ.

Since the produced photon energy is monochromatic, the present photon energy E has one-to-one correspondence to the redshift at the injection z as $E(z) = E_{\rm max}/(1+z)$. Neglecting the intergalactic/interstellar absorption of photons and considering photons produced after the matter-domination, the present CIB energy flux in the flat universe is given by

$$I(E) = E^2 \int dr W(r) = \frac{c}{4\pi} \frac{n_\phi(z) a^3(z)}{\tau_\phi} \frac{E}{H(z)}, \tag{3}$$

where c is the speed of light, $a(z) = (1+z)^{-1}$ is the cosmic scale factor, $H(z)$ is the Hubble parameter at the redshift z, which is related to the present Hubble parameter H_0 through

$$H(z) = H_0 \left(\Omega_\Lambda + \Omega_m (1+z)^3\right)^{1/2}, \tag{4}$$

with Ω_Λ and Ω_m being the dark energy and dark matter density parameter and

$$W(r) \equiv \frac{c}{4\pi} \frac{n_\phi(z) a^3(z)}{\tau_\phi} \frac{dN_\gamma}{dE'}, \tag{5}$$

with $r(z)$ being the comoving distance to the redshift z,

$$r(z) = \int_0^z \frac{c\, dz}{H(z)}, \tag{6}$$

and the photon spectrum at the injection has a delta-function shape in our case:

$$\frac{dN_\gamma}{dE'} = \delta(E' - E_{\rm max}), \tag{7}$$

with $E' = (1+z)E$. Assuming ϕ particles are non-relativistic, we can analytically express its number density at the redshift z as

$$n_\phi(z) = Y_\phi\, s(z) \exp\left(-\frac{t(z)}{\tau_\phi}\right), \tag{8}$$

Y_ϕ as the number-to-entropy density ratio at the high-enough redshift: $Y_\phi \equiv (n_\phi/s)_{t \ll \tau_\phi}$.

where the cosmic time at the redshift z is given by

$$t(z) = \frac{1}{3H_0\sqrt{\Omega_\Lambda}} \ln\left(\frac{\sqrt{\Omega_\Lambda + \Omega_m(1+z)^3} + \sqrt{\Omega_\Lambda}}{\sqrt{\Omega_\Lambda + \Omega_m(1+z)^3} - \sqrt{\Omega_\Lambda}}\right), \tag{9}$$

if the radiation energy density is negligible. The peak energy in the photon spectrum is then found to be

$$E_{\rm peak} \simeq \begin{cases} E_{\rm max} & \text{for } \tau_\phi \gtrsim t_0 \\ E_{\rm max}\left(\frac{3H_0\tau_\phi\sqrt{\Omega_m}}{2}\right)^{2/3} & \text{for } \tau_\phi \lesssim t_0 \end{cases}. \tag{10}$$

An inspection shows that the intensity scales as $I(E) \propto E^{5/2}$ for $E \ll E_{\rm peak}$.

Fig. 1 shows the resulting photon spectrum for several parameter choices. As for cosmological parameters, we take the best-fit values obtained by the Planck satellite [11]. Data points include CIBER [1] with Kelsall zodiac light (ZL) model [12], CIBER with minimum extragalactic background light (EBL) model [1], AKARI [13] and IRTS [14] with only statistical error bars. For the CIBER data with Kelsall ZL model, we also show the range of systematic error. The orange band shows the inferred CIB level from TeV gamma-ray measurements from distant sources by the HESS telescope [15]. The solid line shows the contribution from decaying particle (plus expected background from galaxy counts [16]) for the following parameter set: $E_{\rm max} = 1\,{\rm eV}$, $m_\phi/r_\phi = 3\,{\rm eV}$, $\tau_\phi = 2\times10^{22}\,{\rm sec}$ (upper left), $E_{\rm max} = 1.5\,{\rm eV}$, $m_\phi/r_\phi = 90\,{\rm keV}$, $\tau_\phi = 2.5\times10^{17}\,{\rm sec}$ (upper right) and $E_{\rm max} = 8\,{\rm eV}$, $m_\phi/r_\phi = 80\,{\rm keV}$, $\tau_\phi = 1\times10^{16}\,{\rm sec}$ (lower). For the first parameter set, the lifetime is much longer then the age of the universe and the spectrum shows a sharp cutoff. It is roughly consistent with AKARI and IRTS data at longer wavelength and CIBER with minimum EBL at shorter wavelength. For the second/third parameter set, a significant fraction of ϕ already decayed at the present epoch.[#2] It is consistent with AKARI and IRTS data at longer wavelength and CIBER with Kelsall ZL model at shorter wavelength.

As seen from this figure, taking account of uncertainties of the measured CIB spectrum, relatively broad parameter region is allowed to explain the CIB excess. Several comments and constraints on the parameters are listed below.

- If $\tau_\phi \gtrsim t_0$, the overall flux is determined by the combination $r_\phi/(m_\phi\tau_\phi)$, while the ϕ energy density should be smaller than that of dark matter: $r_\phi \leq 1$ and also we must have $m_\phi \geq 2E_{\rm max}$. Under these conditions the lifetime cannot be longer than $2\times10^{22}\,{\rm sec}$ to explain the CIB excess.

- If $E_{\rm max}$ is larger than $13.6\,{\rm eV}$, photons produced before the reionization epoch contribute to the extra ionizing source. Possible injected energy is severely constrained in such a case [17]. Since we need $E_{\rm peak} \sim 1\,{\rm eV}$ to fit the CIBER/IRTS data, it gives lower bound on the lifetime as $\tau_\phi \gtrsim 10^{16}\,{\rm sec}$.

[#2] Since masses of ϕ and χ are strongly degenerate, the energy density of ϕ (or χ) does not change due to the decay.

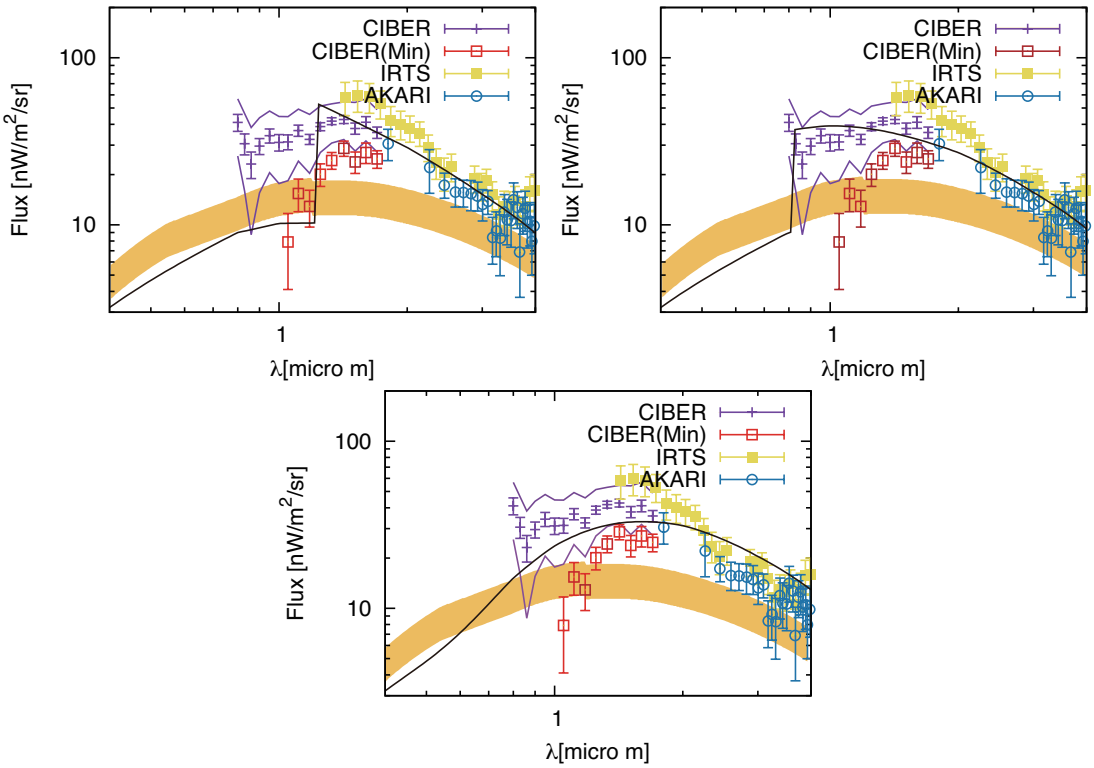


Figure 1: The CIB photon spectrum from decaying particle. Data points include CIBER with Kelsall ZL model, CIBER with minimum EBL model, AKARI and IRTS with only statistical error bars. For the CIBER data with Kelsall ZL model, we also show the range of systematic error. The orange band shows the inferred CIB level by the HESS telescope. The solid line corresponds to the contribution from decaying particle (plus expected background from galaxy counts) for the following parameter set: $E_{\rm max} = 1\,{\rm eV}$, $m_\phi/r_\phi = 3\,{\rm eV}$, $\tau_\phi = 2\times10^{22}\,{\rm sec}$ (upper left), $E_{\rm max} = 1.5\,{\rm eV}$, $m_\phi/r_\phi = 90\,{\rm keV}$, $\tau_\phi = 2.5\times10^{17}\,{\rm sec}$ (upper right) and $E_{\rm max} = 8\,{\rm eV}$, $m_\phi/r_\phi = 80\,{\rm keV}$, $\tau_\phi = 1\times10^{16}\,{\rm sec}$ (lower).

The resultant constraints on the parameter space is schematically shown in Fig. 2. Roughly, we need $10^{16}\,{\rm sec} \lesssim \tau_\phi \lesssim 10^{22}\,{\rm sec}$ and $2\,{\rm eV} \lesssim m_\phi \lesssim 100\,{\rm keV}$.

2.2 Model

Here we briefly discuss possible models to explain the CIB excess, although it will become clear that such models suffer from strong constraints from the CIB anisotropy measurement as shown in the next section.

One may imagine a massive pseudo-scalar particle ϕ, which interacts as

$$\mathcal{L} = -\frac{\phi}{M} F_{\mu\nu}\widetilde{F}^{\mu\nu}. \tag{11}$$

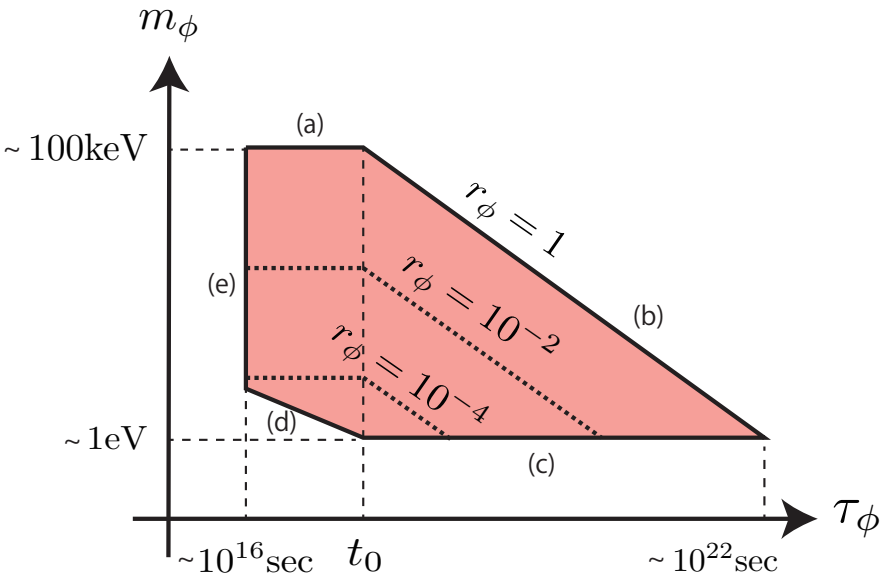


Figure 2: The shaded parameter region on (τ_ϕ, m_ϕ) plane may explain the observed CIB excess. The boundaries are obtained from the consideration about the upper bound on the dark-matter density (a and b), the position of the peak of the CIB spectrum (c and d), and the bound $E_{\rm max} < 13.6$ eV (e). This figure should be regarded as a schematic one, and numerical values written in the figure are also just reference values, not exact one. Dotted lines are contours of r_ϕ to explain the CIB excess.

where $F^{\mu\nu}$ is the field strength tensor of the electromagnetic gauge boson, and M is a constant. With such an interaction, the lifetime of ϕ is given by

$$\tau_\phi = \left(\frac{m_\phi^3}{4\pi M^2}\right)^{-1} \simeq 3 \times 10^{22}\,{\rm sec} \times \left(\frac{1\,{\rm eV}}{m_\phi}\right)^3 \left(\frac{M}{10^9\,{\rm GeV}}\right)^2 . \tag{12}$$

Thus we need $M \lesssim 10^9\,{\rm GeV}$ to explain the CIB excess.[#3] However, such parameter region is already excluded mainly due to too rapid cooling of the horizontal branch stars through the Primakoff process (see, e.g., Ref. [18]). So we do not pursue this possibility further.

If a hidden photon as well as a new pseudo-scalar boson exist, we can avoid the rapid cooling of the horizontal branch stars through the Primakoff process. Let us introduce the following interaction:

$$\mathcal{L} = -\frac{\phi}{M} F_{\mu\nu} \widetilde{F}_H^{\mu\nu}, \tag{13}$$

where $F_H^{\mu\nu}$ is the field strength of the hidden-photon. We assume that there is no kinetic mixing between the photon and hidden photon nor ϕ-γ-γ interaction in the form of Eq. (11).

[#3] In this case, there is an extra factor of 2 in the photon flux (3) since two photons are produced per ϕ decay. Note also that $m_\phi = 2E_{\rm max}$ is almost fixed by the observation and there is no freedom to choose m_ϕ.

In addition, the hidden-photon may acquire mass through the spontaneous breaking of the hidden $U(1)$ symmetry. If ϕ interacts with the standard-model particles only through the interaction (13), Primakoff process is irrelevant.

With the interaction (13), the decay rate of ϕ is given by

$$\Gamma(\phi \to \gamma\gamma_H) = \frac{m_\phi^3}{8\pi M^2}\left(1 - \frac{m_\chi^2}{m_\phi^2}\right)^3 = \frac{E_{\rm max}^3}{\pi M^2}, \tag{14}$$

where γ_H denotes the hidden photon, which takes the role of χ in the previous section, and m_χ is its mass. The rate is independent of the mass of ϕ once we fix $E_{\rm max}$. Thus the lifetime is given by

$$\tau_\phi \simeq 4 \times 10^{21}\,{\rm sec} \times \left(\frac{1\,{\rm eV}}{E_{\rm max}}\right)^3 \left(\frac{M}{10^9\,{\rm GeV}}\right)^2, \tag{15}$$

and it is possible to increase m_ϕ while fixing $E_{\rm max}$ and τ_ϕ by making the ϕ and χ degenerate in mass. Looking at Fig. 2, the allowed parameter region is $10^7\,{\rm GeV} \lesssim M \lesssim 2\times10^9\,{\rm GeV}$ and $2\,{\rm keV} \lesssim m_\phi \lesssim 100\,{\rm keV}$. In this model, there is no Primakoff production of the light boson ϕ and hence the standard constraint from horizontal branch stars is not applied to this coupling. Still, however, there is a plasmon decay process: $\gamma \to \gamma_H\phi$, where the photon obtains an effective mass of the plasma frequency inside the star. It still significantly contributes to the energy loss of the stars as will be shown below.

Now let us discuss the constraints on our model from stellar physics. We closely follow the discussion in Ref. [19]. In the electron plasma, the photon obtains an effective mass ω_P, called the plasma frequency, given by[#4]

$$\omega_P^2 = \frac{4\alpha_e}{\pi}\int dp_e f_e\, p_e \left(v_e - \frac{v_e^3}{3}\right), \tag{16}$$

where α_e is the fine-structure constant, f_e is the electron momentum distribution function, p_e and v_e are the momentum and velocity of the electron. Such a photon with a plasma mass is called plasmon. In the non-relativistic and non-Fermi-degenerate limit, we have

$$\omega_P^2 \simeq \frac{4\pi\alpha_e n_e}{m_e}, \tag{17}$$

with n_e and m_e being the number density and mass of the electron. In the strongly Fermi-degenerate limit, we have

$$\omega_P^2 \simeq \frac{4\pi\alpha_e n_e}{E_F}, \tag{18}$$

[#4] It applies only to the transverse photon. The dispersion relation of longitudinal photon is not a standard form and its behavior is more subtle. Below we only consider the transverse photon.

where E_F denotes the Fermi energy. Thus whenever there is a coupling that causes a decay $\phi \to \chi\gamma$, there must be a plasmon decay process $\gamma \to \phi\chi$ if ϕ and χ are lighter than the plasmon. The plasmon decay rate in the model of (13) is given by

$$\Gamma(\gamma \to \phi\chi) \simeq \frac{\omega_P^3}{8\pi M^2}\frac{\omega_P}{E}, \tag{19}$$

for $\omega_P \gg m_\phi, m_\chi$ where E denotes the incident photon energy and the factor ω_P/E represents the time dilation effect [20]. Note that $E > \omega_P$ is always satisfied from the dispersion relation. Assuming that ϕ and χ escape from the source quickly without trapped by the plasma, the energy loss rate per unit mass is estimated by

$$\epsilon = \frac{1}{\rho_s \pi^2}\int dk k^2 \frac{E}{e^{E/T}-1}\Gamma(\gamma \to \phi\chi), \tag{20}$$

where ρ_s is the mass density of the star. Taking the limit $\omega_p \ll T$, we obtain

$$\epsilon = \frac{\zeta(3)}{4\pi^3}\frac{\omega_p^4 T^3}{\rho_s M^2} \simeq 3\times 10^{-1}\,\mathrm{erg/g/s} \times \left(\frac{\omega_p}{1\,\mathrm{keV}}\right)^4 \left(\frac{T}{10\,\mathrm{keV}}\right)^3 \left(\frac{10^4\,\mathrm{g/cm^3}}{\rho_s}\right)\left(\frac{10^9\,\mathrm{GeV}}{M}\right)^2. \tag{21}$$

Numerical values inside the parenthesis correspond to typical values for the horizontal branch and red giant stars. The constraint reads $\epsilon \lesssim 10\,\mathrm{erg/g/s}$ [19] and hence it may be consistent with the decaying particle scenario to explain the CIB mean intensity excess for $M \sim 10^9\,\mathrm{GeV}$. Moreover, this constraint does not apply to relatively heavy particle: $m_\phi \sim 100\,\mathrm{keV}$. The observation of SN1987A also gives constraint on the extra energy loss rate as $\epsilon \lesssim 10^{19}\,\mathrm{erg/g/s}$. For typical parameters of the supernova core, $\omega_p \sim 10\,\mathrm{MeV}$ [21], $T \sim 30\,\mathrm{MeV}$, $\rho_s \sim 3\times 10^{14}\,\mathrm{g/cm^3}$, the energy loss rate is much smaller than the upper bound.

3 CIB Anisotropy from Decaying Particle

So far we have discussed only the mean CIB intensity from decaying particles. However, since the non-relativistic matter clumps due to the gravitational potential, photons emitted from the matter are not isotropic. Ref. [22] studied the CIB anisotropy from decaying axion-like particle for the axion lifetime much longer than the present age of the universe. We extend the discussion to more general case.

A useful way to discuss the anisotropy is to expand the flux with spherical harmonics $Y_{\ell m}$ as

$$\delta I(E,\Omega) = I(E,\Omega) - \overline{I(E)} = \sum_{\ell,m} a_{\ell m}(E) Y_{\ell m}(\Omega), \tag{22}$$

and define C_ℓ by

$$C_\ell(E) = \left\langle |a_{\ell m}(E)|^2 \right\rangle = \frac{1}{2\ell+1}\sum_{m=-\ell}^{+\ell} |a_{\ell m}(E)|^2. \tag{23}$$

It is calculated as [23]

$$C_\ell(E) = E^4 \frac{2}{\pi} \int dr W(r) \int dr' W(r') \int k^2 dk\, P_\delta(k; r, r') j_\ell(kr) j_\ell(kr'), \tag{24}$$

where $W(r)$ is defined in (5), j_ℓ is the spherical Bessel function and the power spectrum of the matter density fluctuation $\delta(\vec{x}, r)$ is defined as

$$\left\langle \delta_{\vec{k}}(r) \delta_{\vec{k}'}(r') \right\rangle = (2\pi)^3 \delta^3(\vec{k} + \vec{k}') P_\delta(k; r, r'). \tag{25}$$

As for the matter power spectrum, we should take account of the non-linear structure formation effect. It includes the two-halo contribution at large scales and one-halo contribution at small scales. The one-halo term and two-halo terms are written as [24]

$$P_\delta^{\rm 1h}(k, r = r') = \frac{1}{(\rho_m^0)^2} \int dM M^2 \frac{dn(M,z)}{dM} |u_M(k)|^2, \tag{26}$$

and

$$P_\delta^{\rm 2h}(k, r = r') = \left[\frac{1}{\rho_m^0} \int dM M \frac{dn(M,z)}{dM} u_M(k) b(M,z) \right]^2 P_\delta^{\rm (lin)}(k, z), \tag{27}$$

where dn/dM denotes the comoving number density of halo with mass of M, ρ_m^0 is the present matter energy density, $u_M(k)$ denotes the Fourier transform of the density profile of each halo [24], and $P_\delta^{\rm (lin)}(k)$ is the linear matter density perturbation with $b(M, z)$ being the linear halo bias [25]. In the numerical calculation, we use the Sheth-Tormen functional form for dn/dM [26] with the Planck best-fit cosmological parameters [11]. We take the lower cutoff of the halo mass M to be one solar mass in the numerical calculation, but the result is not sensitive to this choice unless the cutoff mass is extraordinarily large. Also we should take the effect of Doppler broadening of the photon spectrum into account. We simply take the injection photon energy spectrum to be the box shape:

$$\frac{dN_\gamma}{dE'} = \begin{cases} (vE_{\rm max})^{-1} & \text{for } |E' - E_{\rm max}| < vE'/2 \\ 0 & \text{otherwise} \end{cases}, \tag{28}$$

where v denotes the typical velocity dispersion of ϕ in the halo.[#5]

We evaluate (24) by the following approximation. First note that the k integration in (24) depends on the shape of $P_\delta(k)$. We are interested in the wave number of $k \gtrsim 0.1\,{\rm Mpc}^{-1}$. In this range, it has nearly flat spectrum below a critical wavenumber $k < k_c$, and it is

[#5] Actually v depends on the halo mass and hence it should be inside the M integral in P_δ. However, for our purpose to show that the anisotropy spectrum significantly exceeds the observed spectrum, it is enough to fix v ($\sim 10^{-3}$) as a representative value in the large halo. Since v is expected to be smaller in small halos and it enhances the anisotropy spectrum, taking account of precise halo dependence of v would make the discrepancy even larger.

proportional to $\sim k^{-2}$ for $k > k_c$ where k_c depends on the redshift z. In such a case, we can approximate the k integration in (24) as

$$\frac{2}{\pi}\int k^2 dk\, P_\delta(k;r,r')j_\ell(kr)j_\ell(kr') \sim \begin{cases} \dfrac{1}{r^2\Delta r_\ell}P(k=k_*;r) & \text{for } |r-r'|<\Delta r_\ell, \\ 0 & \text{otherwise} \end{cases}, \tag{29}$$

where we have defined $\Delta r_\ell = 1/k_*$ and

$$k_* = \max\left[\frac{\ell}{r},\ k_c\right]. \tag{30}$$

It is consistent with the approximation done in Ref. [23] for $\ell/r > k_c$. Second, recall that the function $W(r)$ contains a box-shape function (28) whose width is given by $\Delta r_v \equiv v(1+z)/H(z)$ in terms of the width of the comoving distance r. Hence the effective integration range depends on whether $\Delta r_v > \Delta r_\ell$ or $\Delta r_v < \Delta r_\ell$. If $\Delta r_v > \Delta r_\ell$, we find

$$C_\ell(E) \sim \left(\frac{c}{4\pi}\frac{n_\phi(z)a^3(z)}{\tau_\phi}\frac{E}{H(z)}\right)^2 \frac{\Delta r_\ell}{\Delta r_v}\frac{2\pi^2}{r^2(z)k_*^2}\mathcal{P}_\delta(k=k_*;r(z)), \tag{31}$$

where z is fixed from $E(1+z) = E_{\rm max}$. If, on the other hand, $\Delta r_v < \Delta r_\ell$, we obtain

$$C_\ell(E) \sim \left(\frac{c}{4\pi}\frac{n_\phi(z)a^3(z)}{\tau_\phi}\frac{E}{H(z)}\right)^2 \frac{2\pi^2}{r^2(z)k_*^2}\mathcal{P}_\delta(k=k_*;r(z)). \tag{32}$$

Here $\mathcal{P}_\delta(k) \equiv (k^3/2\pi^2)P_\delta(k)$ denotes the dimensionless power spectrum. The quantity in the first parenthesis represents the mean intensity (3).

Fig. 3 shows the CIB anisotropy spectrum from decaying particle calculated by (31) and (32) at the observation wavelength $\lambda = 1.6\,\mu$m (left) and $\lambda = 0.85\,\mu$m (right). Data points correspond to the HST measurement at the same wavelength [9]. The solid lines show the prediction from decaying particle for the parameter set same as those of Fig. 1, i.e., (a) $E_{\rm max} = 1\,$eV, $m_\phi/r_\phi = 3\,$eV, $\tau_\phi = 2\times10^{22}\,$sec, (b) $E_{\rm max} = 1.5\,$eV, $m_\phi/r_\phi = 90\,$keV, $\tau_\phi = 2.5\times10^{17}\,$sec, (c) $E_{\rm max} = 8\,$eV, $m_\phi/r_\phi = 80\,$keV, $\tau_\phi = 1\times10^{16}\,$sec. For the parameter set (a), there is no contribution to the $0.85\,\mu$m background light at present. We have also taken $v = 4\times10^{-3}$ as a representative value in the largest halo ($M \sim 10^{14}$ times solar mass). It is clearly seen that the predictions exceed the results of HST measurement by orders of magnitude. Although not shown in the figure, it also exceeds the data points from CIBER anisotropy measurement [10]. In the case of (c) the discrepancy is rather mild because the observed photons at the wavelength $\lambda = 1.6\,\mu$m comes from the high redshift due to large $E_{\rm max}$ and the structure formation at the high redshift is relatively suppressed. Even in such a case the predicted anisotropy is far above the observational bound for $\lambda = 0.85\,\mu$m. For larger $E_{\rm max}$ the redshift of the emission epoch becomes larger and the anisotropy is suppressed, but $E_{\rm max}$ is bounded as $E_{\rm max} < 13.6\,$eV so that the ϕ decay does not affect reionization history

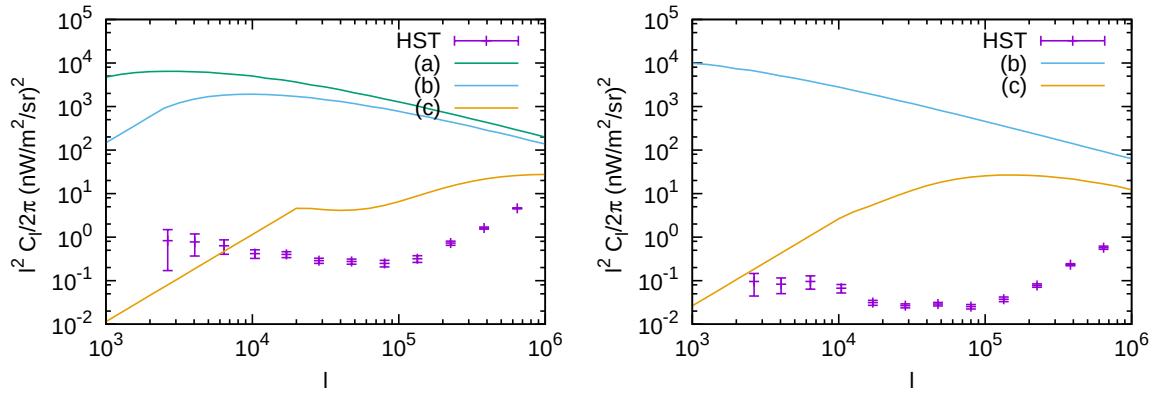


Figure 3: The CIB anisotropy spectrum from decaying particle at the observation wavelength $\lambda = 1.6\,\mu$m (left) and $\lambda = 0.85\,\mu$m (right). Data points correspond to the HST measurement at the same wavelength. The solid lines show the prediction from decaying particle for the parameter set same as those of Fig. 1. (a) $E_{\rm max} = 1\,$eV, $m_\phi/r_\phi = 3\,$eV, $\tau_\phi = 2\times10^{22}\,$sec, (b) $E_{\rm max} = 1.5\,$eV, $m_\phi/r_\phi = 90\,$keV, $\tau_\phi = 2.5\times10^{17}\,$sec, (c) $E_{\rm max} = 8\,$eV, $m_\phi/r_\phi = 80\,$keV, $\tau_\phi = 1\times10^{16}\,$sec.

too much as mentioned in the previous section.[#6] Therefore we conclude that it is difficult for a decaying particle to explain the CIB spectrum excess in the mean intensity without producing too much anisotropy.

4 Conclusions and Discussion

In this paper we considered a possibility that the recent observation of the CIB mean intensity excess by the CIBER experiment as well as the AKARI and IRTS may be explained by decaying light particles. Indeed it is possible to fit the observed CIB spectrum of the mean intensity, but it necessarily predicts too much CIB anisotropy, which contradicts with the anisotropy measurements by the HST and CIBER.

This indicates that the excess CIB radiation may have some astrophysical origin. Here we briefly comment on severe problems of the excess of the diffuse CIB radiation with observed TeV gamma-rays. A TeV gamma-ray scatters off the CIB photon and produces electron and positron through $\gamma+\gamma\to e^-+e^+$. Then the TeV gamma-ray cannot travel from a high-redshifted object such as Active Galactic Nuclei or blazars (with their redshift $z \gg 0.1$). The HESS collaboration reported the upper bound on the flux of the CIB radiation [27] to be consistent with the TeV gamma-ray observations. The value of the CIB radiation flux reported by the CIBER collaboration exceeds this upper bound. In this cir-

[#6] For $10.2\,{\rm eV} < E_{\rm max} < 13.6\,{\rm eV}$, there is another complexity due to the Lyman α absorption, hence we do not consider this energy range.

cumstance, there may exist a non-standard mechanism to solve this problem. For example, the TeV gamma-rays could have origins in line-of-sight cosmic-ray proton interactions with background photons; their continuous gamma-ray productions during their travel may be the source of TeV gamma-rays [28]. This is different from a normal scenario in which the TeV gamma-rays are produced at the sources of the proton acceleration. In such a scenario, the TeV gamma-rays produced at low redshift $z \ll 0.1$ are not absorbed by the CIB radiation and can be observed in the Milky-Way (MW) Galaxy. As another possibility, we may consider models with axion or axion-like particles (ALPs) which mix with the photon when magnetic field exists [29]. We can expect possible oscillations of the TeV gamma-rays into ALPs at around sources utilizing magnetic field. ALPs are not absorbed during their travel from the distant source to the MW Galaxy. We can observe the TeV gamma-rays oscillated-back from ALPs within the MW Galaxy [19, 30, 31, 32].

Acknowledgments

This work is supported by JSPS KAKENHI Grant Numbers 26247042 (K.N. and K.K.), JP15H05889 (K.K.), JP16H0877 (K.K.), JP17H01131 (K.K.), 26400239 (T.M.), 16H06490 (T.M.), 26800121 (K.N.), 26104009 (K.N.), and JP15H05888 (K.N.).

References

[1] S. Matsuura *et al.* [CIBER Collaboration], Astrophys. J. 839, 7 (2017).

[2] A. Franceschini, G. Rodighiero and M. Vaccari, Astron. Astrophys. **487**, 837 (2008) [arXiv:0805.1841 [astro-ph]].

[3] M. R. Santos, V. Bromm and M. Kamionkowski, Mon. Not. Roy. Astron. Soc. **336**, 1082 (2002) [astro-ph/0111467].

[4] R. Salvaterra and A. Ferrara, Mon. Not. Roy. Astron. Soc. **339**, 973 (2003) [astro-ph/0210331].

[5] E. Fernandez and E. Komatsu, Astrophys. J. **646**, 703 (2006) [astro-ph/0508174].

[6] H. Mii and T. Totani, Astrophys. J. **628**, 873 (2005) [astro-ph/0501242].

[7] B. Yue, A. Ferrara, R. Salvaterra and X. Chen, Mon. Not. Roy. Astron. Soc. **431**, 383 (2013) [arXiv:1208.6234 [astro-ph.CO]].

[8] B. Yue, A. Ferrara, R. Salvaterra, Y. Xu and X. Chen, Mon. Not. Roy. Astron. Soc. **433**, 1556 (2013) [arXiv:1305.5177 [astro-ph.CO]].

[9] K. Mitchell-Wynne *et al.*, Nature Commun. **6**, 7945 (2015) [arXiv:1509.02935 [astro-ph.CO]].

[10] M. Zemcov *et al.*, Science **346**, 732 (2014) [arXiv:1411.1411 [astro-ph.CO]].

[11] P. A. R. Ade *et al.* [Planck Collaboration], Astron. Astrophys. **594**, A13 (2016) [arXiv:1502.01589 [astro-ph.CO]].

[12] T. Kelsall *et al.*, Astrophys. J. **508**, 44 (1998) [astro-ph/9806250].

[13] K. Tsumura, T. Matsumoto, S. Matsuura, I. Sakon and T. Wada, Publ. Astron. Soc. Jap. **65**, 121 (2013) [arXiv:1307.6740 [astro-ph.CO]].

[14] T. Matsumoto, M. G. Kim, J. Pyo and K. Tsumura, Astrophys. J. **807**, no. 1, 57 (2015) [arXiv:1501.01359 [astro-ph.GA]].

[15] A. Abramowski *et al.* [H.E.S.S. Collaboration], Astron. Astrophys. **550**, A4 (2013) [arXiv:1212.3409 [astro-ph.HE]].

[16] R. C. Gilmore, R. S. Somerville, J. R. Primack and A. Dominguez, Mon. Not. Roy. Astron. Soc. **422**, 3189 (2012) [arXiv:1104.0671 [astro-ph.CO]].

[17] X. L. Chen and M. Kamionkowski, Phys. Rev. D **70**, 043502 (2004) [astro-ph/0310473].

[18] J. Jaeckel and A. Ringwald, Ann. Rev. Nucl. Part. Sci. **60**, 405 (2010) [arXiv:1002.0329 [hep-ph]].

[19] G. G. Raffelt, "Stars as laboratories for fundamental physics : The astrophysics of neutrinos, axions, and other weakly interacting particles," Chicago, USA: Univ. Pr. (1996) 664 p

[20] G. G. Raffelt, Phys. Rev. D **37**, 1356 (1988).

[21] A. Kopf and G. Raffelt, Phys. Rev. D **57**, 3235 (1998) [astro-ph/9711196].

[22] Y. Gong, A. Cooray, K. Mitchell-Wynne, X. Chen, M. Zemcov and J. Smidt, Astrophys. J. **825**, no. 2, 104 (2016) [arXiv:1511.01577 [astro-ph.CO]].

[23] S. Ando and E. Komatsu, Phys. Rev. D **73**, 023521 (2006) [astro-ph/0512217].

[24] A. Cooray and R. K. Sheth, Phys. Rept. **372**, 1 (2002) [astro-ph/0206508].

[25] D. J. Eisenstein and W. Hu, Astrophys. J. **511**, 5 (1997) [astro-ph/9710252].

[26] R. K. Sheth and G. Tormen, Mon. Not. Roy. Astron. Soc. **308**, 119 (1999) [astro-ph/9901122].

[27] F. Aharonian *et al.* [H.E.S.S. Collaboration], Nature **440**, 1018 (2006) [astro-ph/0508073].

[28] W. Essey, O. Kalashev, A. Kusenko and J. F. Beacom, Astrophys. J. **731**, 51 (2011) [arXiv:1011.6340 [astro-ph.HE]].

[29] G. Raffelt and L. Stodolsky, Phys. Rev. D **37**, 1237 (1988).

[30] D. Hooper and P. D. Serpico, Phys. Rev. Lett. **99**, 231102 (2007) [arXiv:0706.3203 [hep-ph]].

[31] M. A. Sanchez-Conde et al., Phys. Rev. D **79**, 123511 (2009) [arXiv:0905.3270 [astro-ph.CO]].

[32] K. Kohri and H. Kodama, arXiv:1704.05189 [hep-ph].